ACS APPLIED MATERIALS & INTERFACES

Research Article

www.acsami.org

Fabrication of Polypyrrole-Coated Carbon Nanotubes Using Oxidant–Surfactant Nanocrystals for Supercapacitor Electrodes with High Mass Loading and Enhanced Performance

Kaiyuan Shi and Igor Zhitomirsky*

Department of Materials Science and Engineering McMaster University 1280 Main Street West Hamilton, Ontario, Canada L8S 4L7

Supporting Information

ABSTRACT: A conceptually new approach to the fabrication of polypyrrole (PPy)-coated multiwalled carbon nanotubes (MWCNT) for application in electrodes of electrochemical supercapacitors (ES) is proposed. Cetrimonium persulfate $(CTA)_2S_2O_8$ in the form of nanocrystals is used as an oxidant for the chemical polymerization of PPy. Ponceau S (PS) dye is investigated as a new anionic dopant. Testing results show that PS allows reduced PPy particle size and improved electrochemical performance, whereas $(CTA)_2S_2O_8$ nanocrystals promote the formation of PPy nanofibers. We demonstrate for the first time that MWCNT can be efficiently dispersed using $(CTA)_2S_2O_8$ nanocrystals. The analysis of the dispersion mechanism indicates that $(CTA)_2S_2O_8$ dissociation is catalyzed by MWCNT. This new finding opens a new and promising strategy in MWCNT dispersion for colloidal processing of nanomaterials and electrophoretic nanotechnology. Uniformly coated MWCNT are obtained using $(CTA)_2S_2O_8$ as a dispersant for MWCNT and oxidant for PPy polymerization and utilizing advantages of PS as an efficient dopant and nanostructure controlling agent. The analysis of the testing results provides an insight into the influence of PS molecular structure on PPy nanostructure and electrochemical properties. The PPy-coated MWCNT show superior electrochemical performance compared to PPy nanoparticles. The proof-of-principle is demonstrated by the fabrication of ES electrodes with excellent electrochemical performance at high active material loadings, good capacitance retention at high charge–discharge rates, and excellent cycling stability.

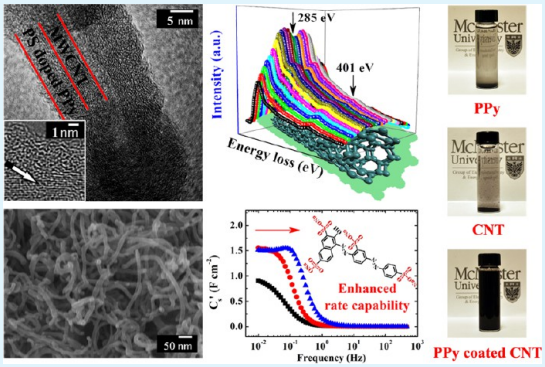

KEYWORDS: *polypyrrole, supercapacitor, carbon nanotube, dopant, coating, nanocrystal*

1. INTRODUCTION

Polypyrrole (PPy) is advanced material for various applications in nanotechnology[1−4] because of its high conductivity, chemical stability, biocompatibility, redox and film forming properties. PPy is under intensive investigation for energy storage in electrochemical supercapacitors (ES). The high specific capacitance (SC) of PPy (theoretical value of 620 F g^{-1}) is attributed to redox reactions, which allow charge storage in the bulk of the electrode.[5] Charge-discharge reactions of PPy require good electrolyte access to the material surface, which can be achieved in porous nanostructured electrodes. A problem, limiting the use of PPy in ES is poor cycling stability.[6,7] It was found that the anion exchange between PPy and electrolyte, variations in the dopant content in the PPy and material swelling during cycling have detrimental effects on SC and cycling stability.[6,8,9]

The development of efficient anionic dopants and new doping mechanisms can address the cycling stability problem. Previous investigations have generated significant interest in the development of efficient dopants for chemical and electrochemical polymerization of PPy. Improved cyclic stability, large voltage window and high electrical conductivity of PPy films were achieved using aromatic dopants.[10,11] The large polyaromatic molecules provided improved cycling stability of the ES electrodes.[11] It was shown that with the variation of the dopant anion, the electrical conductivity of the PPy thin films can differ by three orders of magnitude.[12] In another investigation it was found that the aromatic dopants promoted preferred orientation of pyrrole ring,[13] resulting in anisotropic film growth and enhanced conductivity. The comparison of the experimental data for different aromatic molecules, containing anionic sulfonic groups, showed that conductivity increased with increasing charge/volume ratio of the molecules.[13] Anionic dopants showed significant influence on the size and shape of particles and electrochemical performance of PPy, prepared by chemical polymerization methods.[2,14−16]

Many investigations were focused on the fabrication of PPy nanocomposites, containing carbon nanotubes (CNT) and graphene.[17−21] Such nanocomposites showed high electrical conductivity, improved mechanical and electrochemical proper-

Received: September 25, 2013
Accepted: November 13, 2013
Published: November 13, 2013

 © 2013 American Chemical Society

ties. It was found that the nanocomposite structure is an important factor controlling electrochemical, electrical and mechanical properties. The percolating CNT network allowed reduced volumetric changes of PPy during cycling and improved cycling behavior of the composite materials. The advantages of PPy-CNT composites and PPy-coated CNT have generated significant interest in the development of new methods of their fabrication.[17−20] The major difficulties in the fabrication of PPy-coated CNT are efficient dispersion of CNT during polymerization and control of coating uniformity.

Recent studies highlighted the importance of high materials loading and electrode microstructure for the fabrication of ES devices.[22,23] However, the increase in material loading usually results in increased resistance, limited electrolyte access to the bulk of active material and reduced SC. Thick PPy films showed poor capacitance retention at high charge−discharge rates and poor cycling stability.[24] It was shown that high mass normalized SC (C_m) doesn't necessarily indicate good capacitive behavior.[22] The analysis of area normalized SC (C_s) showed[6] that limited electrolyte access to the bulk of a thick dense film resulted in poor capacitive behavior. Such bulk layer behaved as a capacitor with low capacitance, connected in series with capacitive surface PPy layer, and reduced the total capacitance of the film.

Significant achievements were attained by the fabrication of composites by electrochemical polymerization of polyaniline on a CNT fabric.[25] Pulsed electropolymerization allowed the fabrication of efficient electrodes and cells, which showed excellent electrochemical performance. In our investigation we present an alternative approach to the fabrication of conducting polymer-CNT composites, which is based on colloidal processing and chemical polymerization of PPy.

The goal of this investigation was the fabrication of PPy-multiwalled carbon nanotube (MWCNT) electrodes for ES. New approach is based on the use of $(CTA)_2S_2O_8$ (Scheme 1A), prepared from solutions of cetrimonium bromide (CTAB) and ammonium persulfate ($(NH_4)_2S_2O_8$), as a multifunctional oxidant for chemical polymerization of PPy. The nanocrystals of $(CTA)_2S_2O_8$ allowed excellent dispersion of MWCNT and fabrication of uniformly coated MWCNT. The use of Ponceau S (Scheme 1B) as a new dopant allowed the fabrication of nanostructured PPy with improved electrochemical performance. The porous Ni foam current collectors and MWCNT network allowed good electronic conductivity, improved electrolyte access to the PPy surface and adapted PPy volumetric changes during cycling, resulting in high capacitance, promising cycling life and rate capability for electrodes with high materials loading.

Scheme 1. Chemical Structures of (A) $(CTA)_2S_2O_8$ and (B) Ponceau S

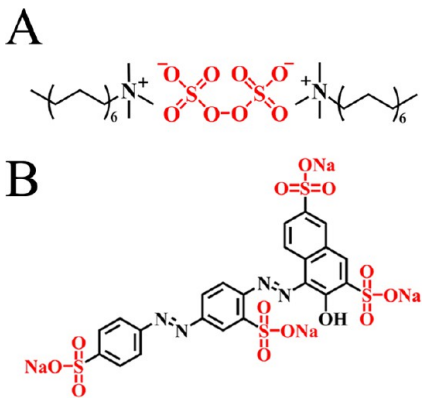

2. EXPERIMENTAL PROCEDURES

2.1. Materials. Ponceau S (PS), cetrimonium bromide (CTAB), ammonium persulfate ($(NH_4)_2S_2O_8$), and pyrrole (Py) were obtained from Sigma-Aldrich company. Py was stored in a refrigerator at 4 °C before the use. MWCNT were obtained from Arkema company. Ni foam (95% porosity) was supplied by Vale company.

For the fabrication of $(CTA)_2S_2O_8$ nanocrystals, 3.64 g (0.01 mol) of CTAB was dissolved in 120 mL of 1 mol L^{-1} HCl solution at 4°C. After being magnetically stirred for 30 min, 1.14 g (0.005 mol) $(NH_4)_2S_2O_8$ was added to the solution and white $(CTA)_2S_2O_8$ precipitate was formed. The reaction was carried out at 4 °C for 20 h. The obtained $(CTA)_2S_2O_8$ precipitate was washed with deionized water using vacuum filtration process and dried in air.

PPy powders were prepared by a chemical polymerization method from the 100 mL solutions, containing 0.05 mol L^{-1} Py monomer and 0−0.025 mol L^{-1} PS dopant, using 0.06 mol L^{-1} of $(NH_4)_2S_2O_8$ or $(CTA)_2S_2O_8$ oxidants for the polymerization reactions. The reactions were carried out at 4 °C for 20 h. The PPy powders were washed with deionized water using vacuum filtration process and dried in air at 70°C.

For the fabrication of PPy-coated MWCNT, the MWCNT were dispersed in water using $(CTA)_2S_2O_8$ as a dispersant. In a typical procedure a 200 mL suspension, containing MWCNT and 0.03 mol L^{-1} $(CTA)_2S_2O_8$ was ultrasonicated for 1 h, cooled down to 4 °C and then a 200 mL solution, containing 0.05 mol L^{-1} of Py and 0.015 mol L^{-1} PS was added. The mass ratio of MWCNT to pyrrole monomer was in the range of 0.11-0.67. The reaction was performed at 4 °C during 20 h. Obtained material was washed with deionized water dried at 70 °C in air.

2.2. Characterization Methods. The adsorption of $(CTA)_2S_2O_8$ on MWCNT was investigated by analyzing the sedimentation test results, electrokinetic properties and Fourier transform infrared spectroscopy(FTIR) data. The limitations of zeta potential concept for the analysis of electrokinetic properties of nanoparticles, containing adsorbed long chain organic molecules, were described in the literature.[26,27] Therefore, the electrokinetic behavior of dispersed MWCNT, containing adsorbed $(CTA)_2S_2O_8$, were investigated by the analysis of electrophoretic deposition (EPD) yield data. EPD was performed from aqueous 1 g L^{-1} MWCNT suspensions, containing 0.1−1 g L^{-1} $(CTA)_2S_2O_8$ or 1 g L^{-1} suspensions of PPy-coated MWCNT without additives. The suspensions were ultrasonicated for 10 min before the EPD. The EPD cell included two Pt electrodes, the distance between the electrodes was 15 mm. The deposition voltage was 20 V. The mass of the deposits was measured after drying in air during 72 h. The deposits were removed from the substrates for the FTIR studies, which were performed using Bio-Rad FTS-40 instrument.

The structure of $(CTA)_2S_2O_8$ was studied by X-ray diffraction (XRD) using powder diffractometer (Nicolet I2, monochromatized CuK_α radiation) at a scanning speed of 0.5° min^{-1}. Electron microscopy studies were performed using a JEOL JSM-7000F scanning electron microscope (SEM) and JEOL 2010F field emission transmission electron microscope (TEM/STEM), equipped with Gatan imaging filter. Element distribution analysis was performed by a combination of high angle annular dark field (HAADF) imaging and electron energy loss spectroscopy (EELS) analysis.

Electrochemical studies were performed using a potentiostat (PARSTAT 2273, Princeton Applied Research). Working electrodes with area of 1 cm^2 were prepared by impregnation of Ni foam with active materials. The counter electrode was a platinum gauze, and the reference electrode was a standard calomel electrode (SCE). Capacitive behavior and electrochemical impedance of the electrodes were investigated in 0.5 M Na_2SO_4 aqueous solutions. Cyclic voltammetry (CV) studies were performed within a potential range of −0.5 to +0.4 V versus SCE at scan rates of 2−200 mV s^{-1}. The

capacitance $C = Q/\Delta V$ was calculated using half the integrated area of the CV curve to obtain the charge (Q), and subsequently dividing the charge by the width of the potential window (ΔV). The specific capacitance $C_m = C/m$ (m = sample mass) and $C_s = C/S$ (S = sample area) were analyzed. The alternating current (AC) complex impedance $Z^* = Z' - iZ''$ was analyzed in the frequency range of 10 mHz-100 kHz at the amplitude of the AC signal of 5 mV. The complex capacitance $C^* = C' - iC''$ was calculated from the impedance data[28] as $C' = Z''/\omega|Z|^2$ and $C'' = Z'/\omega|Z|^2$, where $\omega = 2\pi f$, f = frequency. Two electrodes, containing PPy-coated MWCNT, separated by a porous polyethylene membrane (mean pore size 0.4 μm, Vale, Canada) were used for the fabrication of coin cells (CR2032 type, MTI corporation, U.S.A.), which were sealed using a hydraulic crimping machine (MSK-110, MTI Corporation, U.S.A.). Charge-discharge behaviour of the coin cells was investigated using a battery analyzer (BST8, MTI corporation, U.S.A.).

3. RESULTS AND DISCUSSION

Figure 1 compares the SEM images of PPy powders, prepared using $(NH_4)_2S_2O_8$ and $(CTA)_2S_2O_8$ oxidants. The PPy

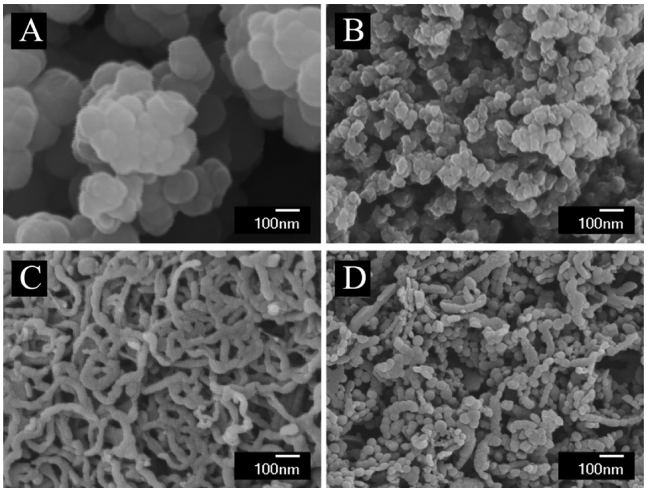

Figure 1. SEM images of PPy powders, prepared from 0.05 mol L^{-1} Py solutions, using (A, B) 0.06 mol L^{-1} $(NH_4)_2S_2O_8$ or (C, D) 0.06 mol L^{-1} $(CTA)_2S_2O_8$ oxidants; (A, C) without PS and (B, D) with 0.015 mol L^{-1} PS.

powder, prepared using $(NH_4)_2S_2O_8$, contained agglomerates of PPy particles with primary particle size of about 100 nm. It is known that PPy, synthesized without dopants, exhibits relatively low conductivity.[29] The use of efficient dopants is important for the development of advanced PPy electrodes for ES. As pointed out above, polyaromatic dopants with high charge to mass ratio are beneficial for the fabrication of PPy with high capacitance, improved cycling stability and high conductivity.

Scheme 1B indicates that PS is a polyaromatic molecule, containing four anionic SO_3^- groups. Therefore, PS is a promising material for application as a new dopant for PPy polymerization. The PPy powder, prepared in the presence of PS (Figure 1B), showed reduced agglomeration and smaller particle size, compared to the PPy powder, prepared without PS (Figure 1A). Significant reduction in particle size was observed with increasing PS concentrations in the range of 0−0.015 mol (Supporting Information Figure S1). It is suggested that anionic PS provided electrostatic repulsion of PPy particles during polymerization, resulting in reduced agglomeration and lower particle size.

SEM studies (Figure 1C) of PPy, prepared using $(CTA)_2S_2O_8$, revealed fibrous morphology of PPy particles. The fabrication of fibrous PPy was reported in other investigations.[30] However, in the previous investigations, Py was added to the CTAB solution[30] before the addition of $(NH_4)_2S_2O_8$ and the CTAB/$(NH_4)_2S_2O_8$ molar ratio of 1:3 was different from that, corresponding to the $(CTA)_2S_2O_8$ stoichiometry. It was suggested[30] that hydrophobic Py molecules were located at the interior of CTAB micelles in aqueous solutions. The addition of $(NH_4)_2S_2O_8$ led to the formation of a CTA^+-Py-$S_2O_8^{2-}$ template, with Py monomers located inside it. The polymerization[30] resulted in the degradation of the template and formation of fibrous PPy. In contrast, in our investigation $(CTA)_2S_2O_8$ was prepared in the form of nanocrystals (Supporting Information Figure S2) before the polymerization. The X-ray diffraction data (Supporting Information FigureS2) showed well-defined diffraction peaks, indicating the formation of a periodic structure, containing CTA^+ and $S_2O_8^{2-}$ bilayers. The typical size of the $(CTA)_2S_2O_8$ nanocrystals was in the range of 5−10 nm (Supporting Information Figure S2). It is important to note that the PPy fibers, shown in Figure 1C, have typical diameters of 25−30 nm and lengths of about 200−500 nm. Therefore, the mechanism, involving the templates, containing Py[30] or other monomers[31] inside or between the CTA layers cannot explain the formation of fibrous PPy, shown in Figure 1C. Note, that in previous investigations[32,33] the dimensions of fibrous PPy corresponded to the dimensions of the templates used. However, the results of our investigation indicated that fibrous PPy can be formed using small nanocrystals of the $(CTA)_2S_2O_8$ oxidant for PPy polymerization.

It is known[34] that $(CTA)_2S_2O_8$ has low solubility in water (1×10^{-5} M). However, the consumption of $S_2O_8^{2-}$ species in the redox reactions with Py monomers resulted in the gradual decomposition of the nanocrystals, containing weakly bonded CTA^+ layers. It is in this regard that the size of CTA^+ is about 2 nm.[35,36] Therefore, the $(CTA)_2S_2O_8$ nanocrystals with typical size of 4-10 nm (Supporting Information Figure S2) contained only 1-2 weakly bonded CTA^+ bilayers. It is not surprising that such small nanocrystals can easily be decomposed in the redox reactions with Py. It is suggested that CTA^+, released from the decomposed $(CTA)_2S_2O_8$ structure, adsorbed on the PPy particles and influenced the PPy particle growth. From the available literature it is known that CTAB is an important shape-controlling surfactant, for the synthesis of nanowires and nanorods.[37−39] It is suggested that layered structure of $(CTA)_2S_2O_8$, containing the layers of $S_2O_8^{2-}$ species, involved in the redox reactions, and CTA^+ layers, promoted the anisotropic nucleation and growth of PPy. The formation of fibers can result from agglomeration of individual PPy nanoparticles, similar to CTAB directed agglomeration of inorganic nanoparticles.[37]

The PPy powders, prepared in the presence of PS and $(CTA)_2S_2O_8$, contained PPy particles of nearly spherical shape (Figure 1D). The size of the particles was about 20-30 nm. However, the powders, prepared in the presence of PS and $(CTA)_2S_2O_8$ also included fibrous particles. Figure 1D indicates that such fibrous particles contained individual spherical particles. This observation supports our suggestion that the mechanism of PPy fibers formation in the presence of $(CTA)_2S_2O_8$ nanoparticles involved the formation of individual PPy nanoparticles and their 1-D agglomeration. The comparison of SEM images shown in Figure 1 and Supporting

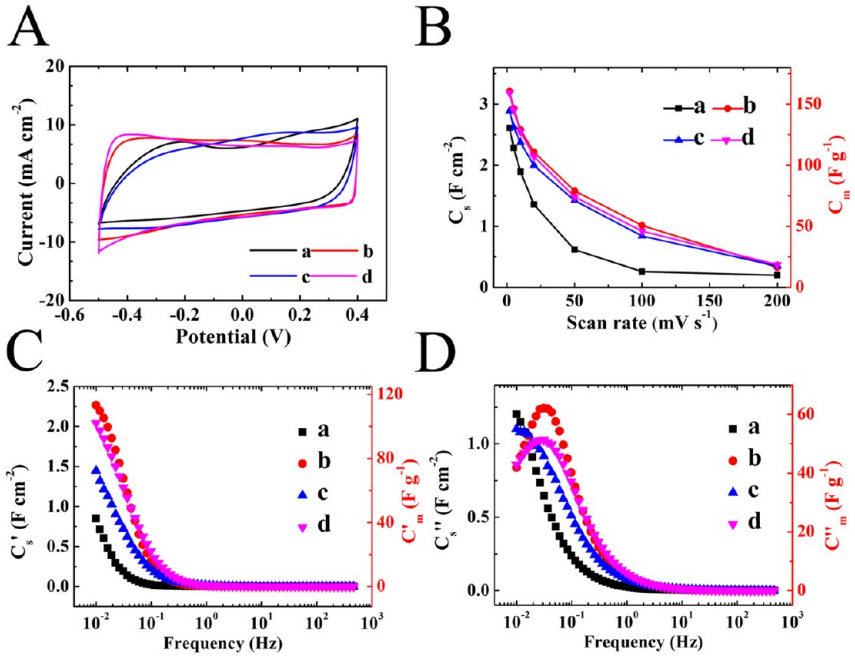

Figure 2. (A) CVs at 2 mV s^{-1}, (B) C_s and C_m versus scan rate, (C) C_s' and C_m', (D) C_s'' and C_m'' versus frequency for 20 mg cm^{-2} PPy electrodes; symbols a, b, c, and d present data for powders, shown in panels A, B, C, and D, respectively, of Figure 1.

Information Figure S1 indicated that PS allowed reduced particle size, however $(CTA)_2S_2O_8$ nanocrystals promoted PPy fiber formation.

The PPy powders were used for the fabrication of ES electrodes. Figure 2A(a−d) presents CV data for the electrodes, prepared from the powders, shown in Figure 1A−D, by chemical polymerization (Scheme 2 and Supporting Information Figure S3 and Scheme S1). The comparison of the CV data revealed the beneficial effect of PS, which allowed nearly box shapes of CVs, indicating improved capacitive behavior (Figure 2A(b,d)). For powders, prepared using $(NH_4)_2S_2O_8$ oxidant, the addition of PS resulted in higher capacitance, especially at high scan rates (Figure 2B(a,b)). The Supporting Information indicates that the increase in the PS concentration in the solutions resulted in the increasing capacitance (Supporting Information Figure S4) and improved capacitance retention at high scan rates. The undoped PPy, prepared using $(CTA)_2S_2O_8$ (Figure 2B(c)), showed higher capacitance, compared to undoped PPy, prepared in the presence of $(NH_4)_2S_2O_8$ oxidant (Figure 2B(a)). Further improvement in the capacitive behavior was achieved by adding PS (Figure 2B(d)). The PPy electrodes (Figure 2B(d)) showed highest C_m and C_s of 159 F g^{-1} and 3.21 F cm^{-2}, respectively at a scan rate of 2 mV s^{-1}. However, the capacitance retention at 200 mV s^{-1} was only 12%.

Scheme 2. (A) Chemical Structure of PS-Doped PPy and (B) Fabrication of PPy-Coated MWCNT

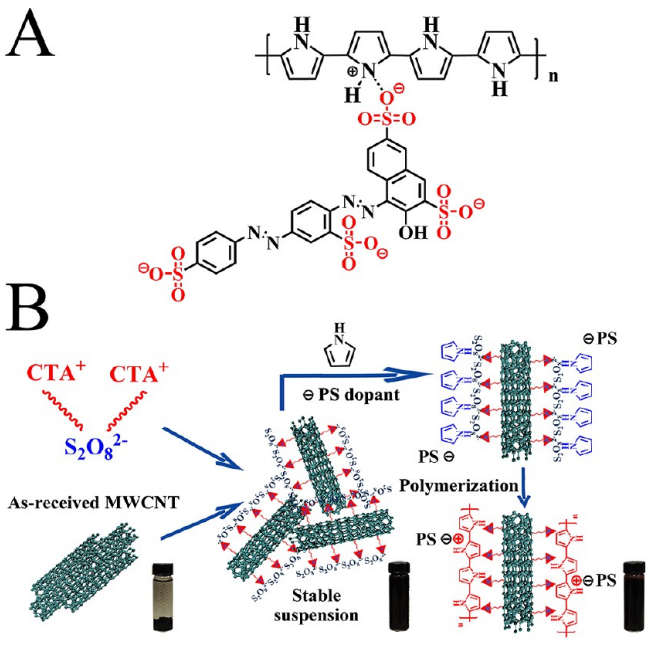

The components of complex AC capacitance $C^* = C' - iC''$, obtained from the impedance $Z^* = Z' - iZ''$ data are plotted in the Figure 2(C,D) versus frequency. The addition of PS resulted in significant increase in C_s' (Figure 2C(a,b)) and reduction in resistance $R = Z'$ (Supporting Information FigureS5(a,b)) for the PPy, prepared using $(NH_4)_2S_2O_8$ oxidant. The C_s' decreased with increasing frequency, indicating relaxation behavior. The C'_s data showed improved capacitance retention at higher frequencies for PS-doped samples, compared to the undoped samples (Figure 2C and Supporting Information FigureS6). The iC_s'' versus frequency plot for PS-doped sample showed a typical relaxation maximum (Figure 2D(b)). The relaxation frequency increased and resistance $R = Z'$ decreased with increasing dopant concentration in the solutions, used for the chemical polymerization (Supporting Information FigureS6 and Table S1). The undoped PPy electrodes, prepared using $(CTA)_2S_2O_8$, showed higher C_s', improved capacitance retention at higher frequencies and reduced R, compared to the electrodes prepared using $(NH_4)_2S_2O_8$ oxidant (Figure 2C(c), Supporting Information FigureS5). Further improvement in the capacitive behavior was achieved using PS dopant (Figure 2C(d),D(d) and Supporting Information Figures S5 and S6). Scheme 2A shows a structure

dx.doi.org/10.1021/am404159b | ACS Appl. Mater. Interfaces 2013, 5, 13161−13170

of PPy, doped with PS. It is known that PPy chain has a positive charge every 3−4 units.[14,40] The charge is counterbalanced by an anionic dopant.[40] It is important to note that PS has four SO_3^- groups, which can compensate four positive charges of different units of one chain or different chains (Supporting Information Figure S3A). It is known that dopants with multiple negative charges, compensating positive charges of different units, can improve conductivity and other properties of PPy.[41] The polymerization reaction for PPy in the presence of $(NH_4)_2S_2O_8$ oxidant was described in the literature.[2] A similar reaction can be suggested for PPy polymerization in the presence of $(CTA)_2S_2O_8$ oxidant (Supporting Information Figure S3B).

It is important to note that the development of efficient ES for high power applications requires good capacitive behavior at high scan rates and high AC frequencies. The improved capacitance retention of electrodes at high charge−discharge rates can be achieved by the use of PPy-coated MWCNT. Our new strategy was based on the use of $(CTA)_2S_2O_8$ nanocrystals for the dispersion of MWCNT and fabrication of PPy-coated MWCNT (Scheme 2). Difficulties in the formation of PPy coatings on MWCNT are attributed to poor dispersibility of MWCNT in water and low suspension stability. However, sedimentation tests showed that the MWCNT suspensions, containing $(CTA)_2S_2O_8$ were stable for more than one month. The dispersion mechanism was also analyzed using EPD method. It was not possible to deposit films by EPD from 0.5−1 g L^{-1} MWCNT or 0.5−1 g L^{-1} $(CTA)_2S_2O_8$ suspensions. However, cathodic deposits were obtained from 1 g L^{-1} MWCNT suspensions, containing $(CTA)_2S_2O_8$. The deposition yield increased with increasing $(CTA)_2S_2O_8$ concentration in the suspensions and deposition time (Figure 3A,B). The method resulted in the formation of continuous films (Figure 3A, inset). The decrease in the deposition rate with increasing deposition time (Figure 3B) can be attributed to the decreasing

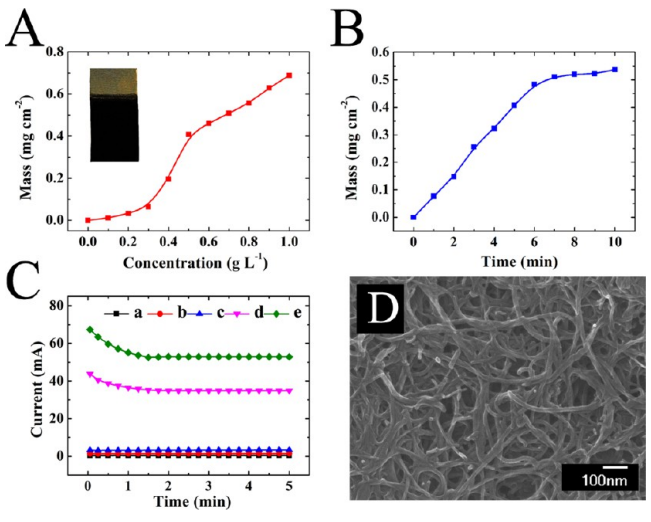

Figure 3. (A, B) Deposit mass for 1 g L^{-1} MWCNT suspension versus (A) $(CTA)_2S_2O_8$ concentration at a deposition time of 5 min (inset shows a MWCNT film on stainless steel) and (B) deposition time at $(CTA)_2S_2O_8$ concentration of 0.5 g L^{-1}; (C) deposition current versus deposition time for (a) 1 g L^{-1} MWCNT, (b) 0.5 g L^{-1} $(CTA)_2S_2O_8$, (c) 1 g L^{-1} $(CTA)_2S_2O_8$, (d) 1 g L^{-1} MWCNT and 0.5 g L^{-1} $(CTA)_2S_2O_8$, and (e) 1 g L^{-1} MWCNT and 1 g L^{-1} $(CTA)_2S_2O_8$ suspensions; (D) SEM image of a film obtained from 1 g L^{-1} MWCNT and 1 g L^{-1} $(CTA)_2S_2O_8$ suspension.

electric field in the suspension due to increasing voltage drop in the growing deposit.[42] The formation of cathodic deposits indicated that MWCNT were positively charged in the suspensions. The results of electric current measurements during EPD at a constant voltage provided important information related to the charging and dispersion mechanism. Electric current in the 1 g L^{-1} MWCNT, 0.5 g L^{-1} $(CTA)_2S_2O_8$ and 1 g L^{-1} $(CTA)_2S_2O_8$ suspensions was very low (Figure 3C). As pointed out above, no deposit formation was achieved from such suspensions. However, the addition of 1 g L^{-1} MWCNT to 0.5 g L^{-1} $(CTA)_2S_2O_8$ or 1 g L^{-1} $(CTA)_2S_2O_8$ suspensions resulted in significant increase in electric current (Figure 3C). The starting current in the mixed 1 g L^{-1} MWCNT and 1 g L^{-1} $(CTA)_2S_2O_8$ suspensions was at least 20 times higher compared to the currents in the suspensions of individual components. The decrease in current with time (Figure 3C(d,e)) is related to the decreasing electric field in the suspensions due to increasing voltage drop in the growing films. SEM images of the films showed a continuous network of MWCNT(Figure 3D).

It is known that electrode reactions are not involved in the EPD process.[43] As pointed out above, the solubility of $(CTA)_2S_2O_8$ in water is very low. It is suggested that $(CTA)_2S_2O_8$ nanocrystals were adsorbed on the MWCNT and dissociation of $(CTA)_2S_2O_8$ nanoparticles was catalyzed by MWCNT. The MWCNT catalyzed dissociation of $(CTA)_2S_2O_8$ nanoparticles resulted in increasing ionic strength of the suspensions, as indicated by high starting current and high current during EPD (Figure 3C(d,e)). It is suggested that CTA^+ species were adsorbed on MWCNT, providing electrosteric stabilization and positive charge for cathodic EPD. The CTA^+ and $S_2O_8^{2-}$ species formed an electrical double layer (Scheme 2B). The CTA^+ adsorption on MWCNT was confirmed by FTIR studies (Supporting Information Figure S7).

The addition of Py to the suspensions, stabilized with CTA^+ and $S_2O_8^{2-}$ species, resulted in the oxidation of Py by the $S_2O_8^{2-}$ in the double layer, polymerization and formation of PPy coatings. The suspensions of coated MWCNT, prepared using $(CTA)_2S_2O_8$ nanoparticles in the presence of PS, were stable for more than one month after fabrication(Supporting Information Figure S8). The PPy-coated MWCNT were positively charged in the suspensions and formed cathodic films by EPD (Supporting Information Figure S9) without any additives. In contrast, the suspensions prepared using $(NH_4)_2S_2O_8$ instead of $(CTA)_2S_2O_8$ showed precipitation after 12 h (Supporting Information Figure S8). The good dispersion of PPy-coated MWCNT is not related to PPy coating, because PPy particles, prepared without MWCNT using $(CTA)_2S_2O_8$, showed precipitation after 48 h (Supporting Information Figure S8). It is suggested that colloidal stability of PPy-coated MWCNT, prepared using $(CTA)_2S_2O_8$, is related to adsorbed CTA^+, which provided electrosteric dispersion.

The use of $(CTA)_2S_2O_8$ nanoparticles offered many advantages for MWCNT dispersion and fabrication of PPy coatings on MWCNT. A critical property of a dispersant is its adsorption on a particle surface. Adsorbed dispersant provides particle dispersion, however non-adsorbed dispersant acts as an electrolyte.[26] The non-adsorbed ionic dispersant increases the ionic strength of the suspensions and promotes particle flocculation in agreement with the DLVO theory.[26] Therefore, a dispersant must be adsorbed on the particles and the

concentration of non-adsorbed dispersant must be minimized. Because of the low solubility of $(CTA)_2S_2O_8$, the ionic concentration of $(CTA)_2S_2O_8$ solutions was low. The interaction of $(CTA)_2S_2O_8$ nanocrystals with MWCNT resulted in adsorption of CTA^+ on the MWCNT surface. As a result, efficient dispersion and EPD of MWCNT was achieved at $(CTA)_2S_2O_8$/MWCNT mass ratio of 0.5. It is in this regard that relatively high concentrations of CTAB were used for the dispersion of CNT.[44−47] It was found that optimum CTAB concentration for the dispersion of CNT is slightly higher than critical micelle concentration and the optimum CTAB/CNT ratio was found to be about 7 at such CTAB concentration.[44] It is known[48] that the formation of micelles reduces suspension stability, because osmotic pressure of the surfactant micelles promotes CNT agglomeration.

The results of electron microscopy investigations, presented below, indicated that use of $(CTA)_2S_2O_8$ in the form of nanocrystals as a dispersant for MWCNT and oxidant for Py polymerization allowed the fabrication of PPy-coated MWCNT. Moreover, the results indicated that the use of nanocrystals, containing CTA^+ species, for the dispersion and deposition of pristine or coated MWCNT opens new and promising strategies in colloidal processing of nanomaterials, including EPD nanotechnology of thin films. It should be noted that the fabrication of PPy-coated MWCNT by other methods, involved functionalization of MWCNT in hot concentrated acids (HNO_3 at 80°C[17] or H_2SO_4/ HNO_3 mixture at 90 °C[18]) in order to achieve dispersion. However, for applications based on conductive properties of MWCNT, the oxidation of MWCNT in acids must be avoided. In our strategy, pristine MWCNT were well dispersed before and after polymerization. The $S_2O_8^{2-}$ species in the double layer at the MWCNT surface provided a template for the uniform coating.

The PPy-coated MWCNT were investigated by electron microscopy. It was found that the formation of PPy-coated MWCNT is influenced by $(CTA)_2S_2O_8$ and PS. The SEM and TEM images of powders, prepared without PS are shown in Figure 4(A,B) and Figure 5(A,B). The powders, prepared using $(CTA)_2S_2O_8$ contained PPy-coated MWCNT and PPy fibers

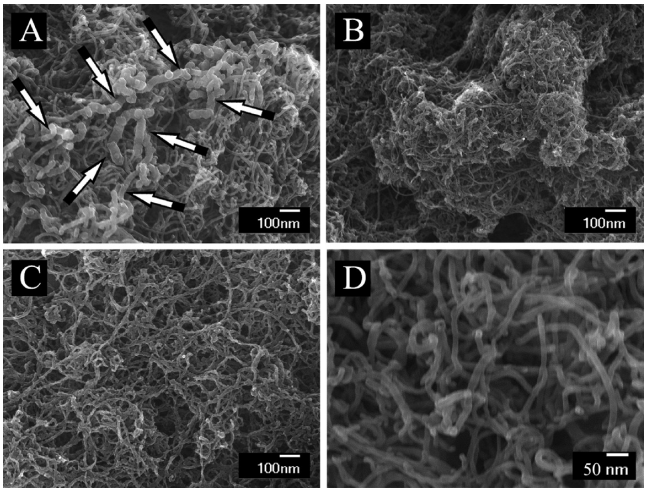

Figure 4. SEM images of PPy-MWCNT powders prepared using (A) $(CTA)_2S_2O_8$ (arrows show PPy fibers), (B) PS and $(NH_4)_2S_2O_8$, (C, D) PS and $(CTA)_2S_2O_8$ at different magnifications. Concentrations of Py, PS, $(NH_4)_2S_2O_8$, and $(CTA)_2S_2O_8$ were the same as in Figure 1, mass ratio MWCNT/Py = 3:7.

(Figures 4A and 5A). The use of $(NH_4)_2S_2O_8$ as an oxidant resulted in the formation of highly agglomerated particles, containing MWCNT and PPy (Figure 4B and Figure 5B). Uniformly coated MWCNT were obtained when Py and PS were added to the MWCNT suspensions, containing $(CTA)_2S_2O_8$ (Figures 4C, D and 5C, D). This result indicated that PS prevented the formation of fibrous PPy in the bulk of the suspensions. The formation of PPy-coated MWCNT was confirmed by the analysis of high magnification TEM images (Figure 5D). Figure 5D shows typical TEM image of PPy-coated MWCNT and inset shows the PPy-MWCNT interface. The SEM images (Figure 4C, D) and TEM images (Figure 5C, D) indicated the formation of nonagglomerated and uniformly coated MWCNT with coating thickness of about 5 nm. The results of EELS studies were presented in Figure 5E, F. Line scans were performed by rastering the electron beam in a line perpendicular to the PPy-coated MWCNT in 0.5 nm steps, measuring the spectrum for each step (Figure 5E).

The spectra in the energy range of 250−500 eV showed both the C−K and N−K edges at about 285 and 401 eV, respectively. The elemental distribution profile for nitrogen has a saddle shape with two maxima on both sides of the MWCNT, related to PPy coating(Figure 5F). The carbon dominates in the middle of the profile with two small maxima from the both sides due to the hollow structure of MWCNT and PPy coating (Figure 5F). The results of SEM, TEM and EELS data, coupled with the results of FTIR studies (Supporting Information Figure S10) indicated the formation of PPy-coated MWCNT. The interaction of PPY and MWCNT is mainly related to $\pi-\pi$ interaction mechanism. The important factor, controlling the formation of PPy coatings was the MWCNT:Py ratio in solutions (Figure 6 and Supporting Information FigureS11). When MWCNT/Py ratio was 1:9 the coatings were non-uniform(Figure 6). The uniformity improved when the ratio was 2:8. Uniformly coated MWCNT were obtained at MWCNT/Py ratio of 3:7 (Figure 6). Further increase in the MWCNT content in the solutions resulted in reduced coating thickness and formation of uncoated areas of MWCNT (Supporting Information Figure S11).

The use of PPy-coated MWCNT allowed significant improvement in capacitance retention at high scan rates. Figure 7A, B, C presents CVs for the electrodes, prepared using powders shown in Figure 5A, B, C. The larger CV area for the PPy electrodes, prepared using $(CTA)_2S_2O_8$ and PS, indicates higher capacitance. The investigation of the capacitance, calculated from the CV data, showed capacitance retention of 63% at a scan rate of 200 mV s^{-1}. Moreover, relatively high capacitance of 1.4 F cm^{-2} (72 F g^{-1}) was achieved at a scan rate of 200 mV s^{-1}. The capacitance, calculated from the impedance data (Supporting Information Figure S12) was plotted versus AC frequency in Figure 7E, F. The C_s' data showed relaxation behavior (Figure 7E), as indicated by the rapid decrease in the C_s' above relaxation frequencies, which correspond to the frequencies of C_s'' maxima (Figure 7F). The comparison of the data presented in Figures 2C, D and 7E, F showed that the use of PPy-coated MWCNT allowed significant improvement in capacitance retention at high AC frequencies.

Moreover, the electrodes, containing PPy-coated MWCNT showed reduced resistance R (Supporting Information Figure S12).The PPy-coated MWCNT, prepared in the presence of $(CTA)_2S_2O_8$ and PS, showed significantly higher C_s' in the frequency range below 1 Hz, compared to PPy powders (Figure

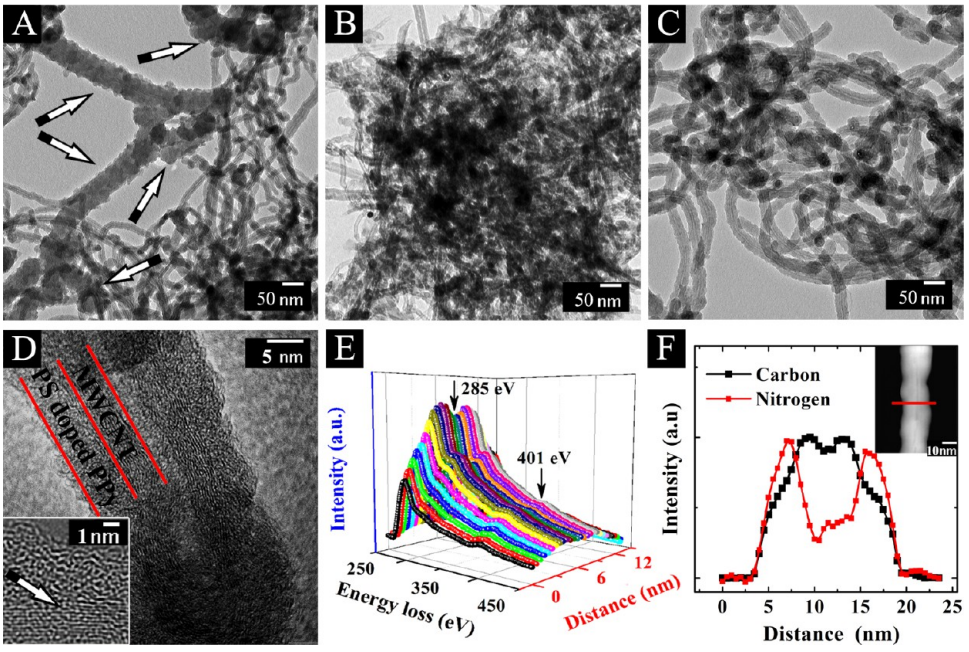

Figure 5. TEM images of PPy-MWCNT powders prepared using (A) $(CTA)_2S_2O_8$ (arrows show PPy fibers), (B) PS and $(NH_4)_2S_2O_8$, and (C, D) PS and $(CTA)_2S_2O_8$ at different magnifications. Arrow in the inset of panel D shows HRTEM image of PPy-MWCNT interface. (E) Set of resolved EELS spectra measured along a line across PPy-coated MWCNT. (F) Element distribution obtained from the EELS data. Inset shows HAADF image of a region for analysis. concentrations of Py, PS, $(NH_4)_2S_2O_8$, and $(CTA)_2S_2O_8$ were the same as in Figure 1, mass ratio MWCNT/Py = 3:7.

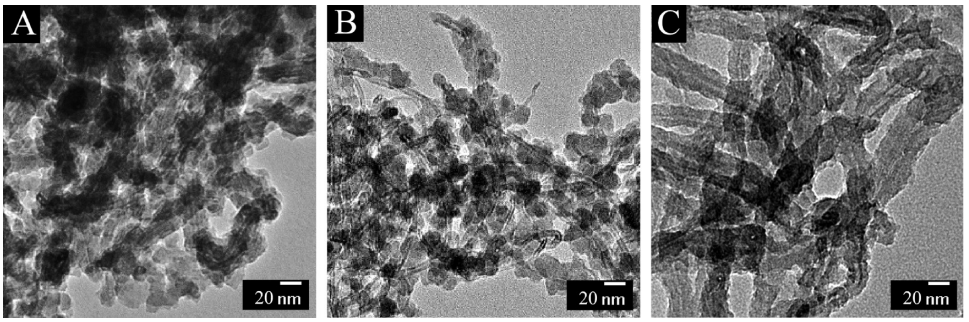

Figure 6. TEM images of PPy-coated MWCNT, prepared from 0.05 mol L^{-1} Py solutions, using 0.06 mol L^{-1} $(CTA)_2S_2O_8$ and 0.015 mol L^{-1} PS, mass ratio MWCNT/Py (A) 1:9, (B) 2:8, and (C) 3:7.

2C, D) and the relaxation maximum shifted to 293 mHz (Figure 7E(c), F(c)).

Previous investigations[49,50] showed that specific capacitances of conductive polymers, calculated from the AC impedance data are significantly lower, compared to the capacitances, calculated from the CV data. Such data analysis is usually performed at the same time scale, because the voltammetric capacitance depends on a scan rate, whereas AC capacitance depends on frequency.[49] It was suggested that some "deeply trapped" dopant counterions can be immobile at low AC voltages.[50] Such ions can be released at higher voltages in CV experiments and contribute to higher capacitance. In other investigations the discrepancy between the AC and voltammetric capacitances was attributed to chemical and physical heterogeneity and existence of sites with wide range of redox potentials.[49,51,52] However, the comparison of our experimental data at the same time scale showed that $C_s' = 1.50$ F cm^{-2} at 110 mHz was close to the $C_s = 1.45$ F cm^{-2} measured at a scan rate of 200 mV/s for the full scan in a voltage window of 0.9 V (Figure 7D(c) and 7E(c)).

The advantages of PPy-coated MWCNT are also evident from the capacitance versus electrode mass dependencies, presented in Figure 8 and additional detailed information presented in Supporting Information Figures S13 and S14 for electrodes of different mass and with different MWCNT content. The specific capacitance $C_s(2)$ and $C_s(100)$, measured at scan rates of 2 and 100 mV s^{-1}, respectively increased with increasing materials loading, indicating good utilization of the electrode material. In contrast, the electrodes, prepared without PS or with $(NH_4)_2S_2O_8$ oxidant showed lower capacitance, and no increase in C_s was observed with increasing material loading above 20 mg cm^{-2}. The highest $C(2)_s$ of 4.1 F cm^{-2} was obtained for active material loading of 35 mg cm^{-2} for electrode density of 1.3 g cm^{-3}. Moreover, remarkably high $C(100)_s$ of 2.8 F cm^{-2} was obtained. The electrodes, containing PPy-coated MWCNT, showed capacitance retention of 94.4% after 1000 cycles (Figure 9A). The shape of the CV(Figure 9A, inset) and resistance value $R = Z'$ (Figure 9B) remained practically unchanged during cycling. The 6% decrease in the C_s' after 1000 cycles (Figure 9C) correlated with corresponding reduction in C_s, obtained from the CV data (Figure 9A).

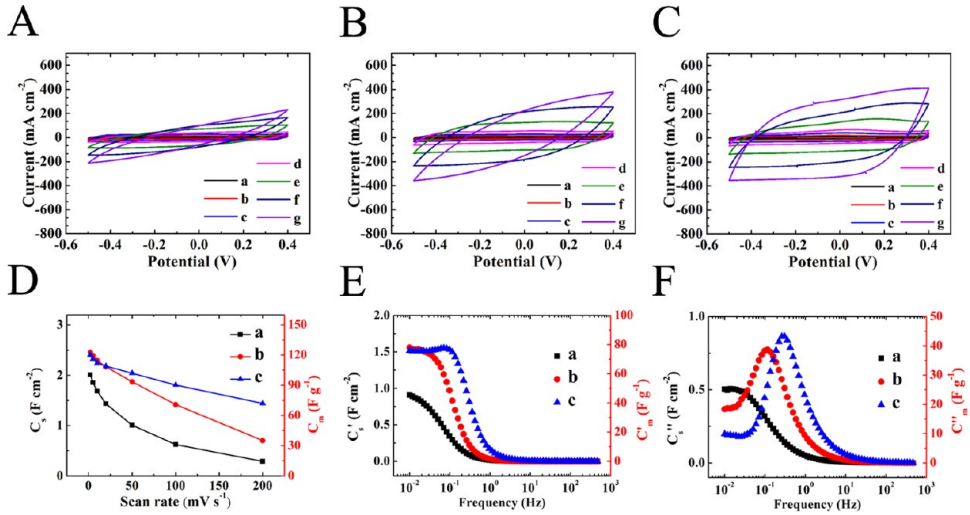

Figure 7. (A, B, C) CVs at scan rates of (a) 2, (b) 10, (c) 50, (d) 100, and (e) 200 mV s^{-1}. (D) C_s and C_m versus scan rate. (E) C_s' and C_m' and (F) C_s'' and C_m'' versus AC frequency. Panels A, B, and C and symbols a, b, and c in panels D and F present data for powders shown in panels A, B, and C of Figure 5, respectively, for electrode mass of 20 mg cm^{-2}.

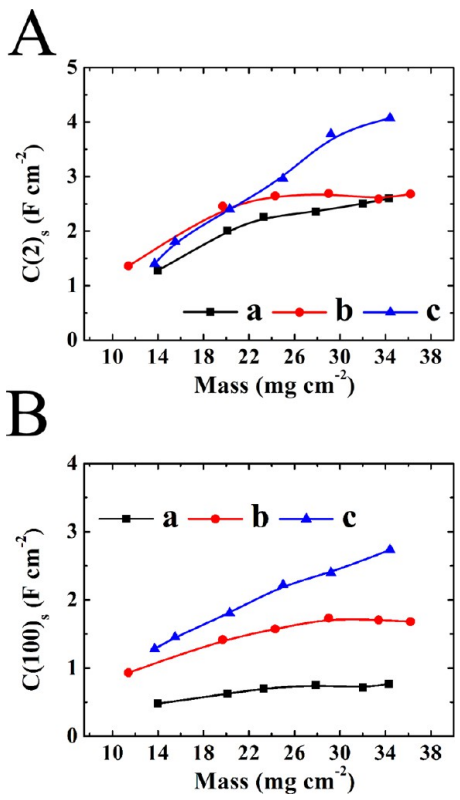

Figure 8. C_s versus electrode mass obtained at scan rates of (A) 2 and (B) 100 mV s^{-1}. Symbols a, b, and c present data for powders shown in panels A, B, and C of Figure 5, respectively.

However, no changes in the relaxation frequency were observed during cycling (Figure 9D). The results indicated that the use of PPy-coated MWCNT, prepared using $(CTA)_2S_2O_8$ nanocrystals, which served as a dispersant and oxidant, and PS as a new anionic dopant, allowed the fabrication of electrodes with high capacitance, high material loading, good capacitance retention at high scan rates and good cycling stability. The electrodes were used for the fabrication of coin cell modules, which showed good electrochemical performance (Supporting Information Figure S15–S17) and powered 20 mA light emitting devices (Supporting Information Figure S15). The comparison of the testing results with the literature data[25] for the polyaniline-CNT fabric composites, prepared by electropolymerization, and tested in H_2SO_4 electrolyte, indicated that the alternative colloidal method based on the chemical polymerization of PPy, allowed comparable electrochemical performance and good cycling stability using Na_2SO_4 electrolyte at high materials loadings.

4. CONCLUSIONS

PS was used as a new anionic dopant and $(CTA)_2S_2O_8$ nanocrystals were used as an oxidant for PPy polymerization. Testing results demonstrated that PS allowed reduced PPy particle size and improved electrochemical performance, whereas $(CTA)_2S_2O_8$ nanocrystals promoted the formation of PPy nanofibers. The PPy powders prepared using PS and $(CTA)_2S_2O_8$ nanocrystals showed improved electrochemical performance for application in ES, however the PPy-coated MWCNT showed superior electrochemical performance compared to PPy nanoparticles. It was found that $(CTA)_2S_2O_8$ nanocrystals can be used for efficient dispersion and EPD of MWCNT. The $(CTA)_2S_2O_8$ dissociation was catalyzed by MWCNT. In this approach efficient dispersion was achieved at low CTA^+ concentration. The use of $(CTA)_2S_2O_8$ nanocrystals as a dispersant for MWCNT and oxidant for PPy and the use of PS as an anionic dopant and PPy structure controlling agent allowed the fabrication of uniformly coated MWCNT. The PPy-coated MWCNT showed excellent dispersibility. The method allowed the fabrication of ES electrodes with high materials loading, excellent capacitance retention at high charge–discharge rates and excellent cycling stability. The highest C_s of 4.1 F cm^{-2} was obtained at a scan rate of 2 mV s^{-1} for material loading of 35 mg cm^{-2}. The PPy-coated MWCNT is a promising material for ES application. The method developed in this investigation can be used for the surface modification of MWCNT with other functional materials and fabrication of nanomaterials by colloidal methods and thin films by EPD.

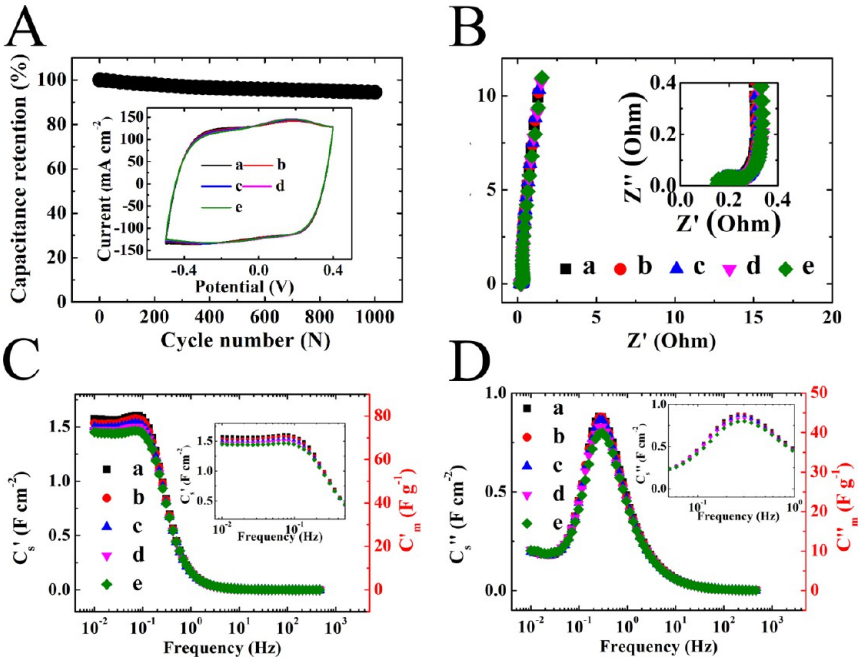

Figure 9. (A) Capacitance retention versus cycle number; inset shows corresponding CVs at 50 mV s^{-1}. (B) Nyquist plot of complex impedance; inset shows high frequency range. (C) C_s' and C_m' and (D) C_s'' and C_m'' versus frequency. Insets in panels C and D show low frequency range, after (a) 1st, (b) 250th, (c) 500th, (d) 750th, and (e) 1000th cycles for 20 mg cm^{-2} electrodes, prepared from powder shown in Figure 5C.

■ ASSOCIATED CONTENT

Ⓢ Supporting Information

Chemical structure of PS-doped PPy, SEM and TEM images of PPy powders and nanofibers, XRD and FTIR data, EPD yield data, and electrochemical testing results. This information is available free of charge via the Internet at http://pubs.acs.org/.

■ AUTHOR INFORMATION

Corresponding Author

*E-mail: zhitom@mcmaster.ca. Phone: 1-(905) 525-9140.

Notes

The authors declare no competing financial interest.

■ ACKNOWLEDGMENTS

The authors gratefully acknowledge the financial support of the Natural Sciences and Engineering Research Council of Canada

■ REFERENCES

(1) Romero, I. S.; Schurr, M. L.; Lally, J. V.; Kotlik, M. Z.; Murphy, A. R. *ACS Appl. Mater. Interfaces* **2013**, *5*, 553−564.
(2) Qie, L.; Yuan, L.-X.; Zhang, W.-X.; Chen, W.-M.; Huang, Y.-H. *J. Electrochem. Soc.* **2012**, *159*, A1624−A1629.
(3) Wei, L.; Sevilla, M.; Fuertes, A. B.; Mokaya, R.; Yushin, G. *Adv. Funct. Mater.* **2012**, *22*, 827−834.
(4) Li, W.; Qiu, T.; Wang, L.; Ren, S.; Zhang, J.; He, L.; Li, X. *ACS Appl. Mater. Interfaces* **2013**, *5*, 883−891.
(5) Snook, G. A.; Kao, P.; Best, A. S. *J. Power Sources* **2011**, *196*, 1−12.
(6) Shi, K.; Zhitomirsky, I. *J. Power Sources* **2013**, *240*, 42−49.
(7) Pyo, M.; Reynolds, J. R.; Warren, L. F.; Marcy, H. O. *Synth. Met.* **1994**, *68*, 71−77.
(8) Cohen, Y.; Levi, M.; Aurbach, D. *Langmuir* **2003**, *19*, 9804−9811.
(9) Sharma, R.; Rastogi, A.; Desu, S. *Electrochem. Commun.* **2008**, *10*, 268−272.
(10) Hakansson, E.; Lin, T.; Wang, H.; Kaynak, A. *Synth. Met.* **2006**, *156*, 1194−1202.
(11) Lang, X.; Wan, Q.; Feng, C.; Yue, X.; Xu, W.; Li, J.; Fan, S. *Synth. Met.* **2010**, *160*, 1800−1804.
(12) Wang, P.-C.; Yu, J.-Y. *React. Funct. Polym.* **2012**, *72*, 311−316.
(13) Mitchell, G. R.; Davis, F. J.; Legge, C. H. *Synth. Met.* **1988**, *26*, 247−257.
(14) Han, M.; Chu, Y.; Han, D.; Liu, Y. *J. Colloid Interface Sci.* **2006**, *296*, 110−117.
(15) Wang, Y.; Yang, C.; Liu, P. *Chem. Eng. J.* **2011**, *172*, 1137−1144.
(16) Goel, S.; Mazumdar, N. A.; Gupta, A. *Polym. Adv. Technol.* **2010**, *21*, 205−210.
(17) Han, Y.; Shen, M.; Lin, X.; Ding, B.; Zhang, L.; Tong, H.; Zhang, X. *Synth. Met.* **2012**, *162*, 753−758.
(18) Sahoo, N. G.; Jung, Y. C.; So, H. H.; Cho, J. W. *Synth. Met.* **2007**, *157*, 374−379.
(19) Hughes, M.; Chen, G. Z.; Shaffer, M. S.; Fray, D. J.; Windle, A. H. *Chem. Mater.* **2002**, *14*, 1610−1613.
(20) Fang, Y.; Liu, J.; Yu, D. J.; Wicksted, J. P.; Kalkan, K.; Topal, C. O.; Flanders, B. N.; Wu, J.; Li, J. *J. Power Sources* **2010**, *195*, 674−679.
(21) Shi, K.; Zhitomirsky, I. *J. Colloid Interface Sci.* **2013**, *407*, 474−481.
(22) Gogotsi, Y.; Simon, P. *Science* **2011**, *334*, 917−918.
(23) Guillemet, P.; Brousse, T.; Crosnier, O.; Dandeville, Y.; Athouel, L.; Scudeller, Y. *Electrochim. Acta* **2012**, *67*, 41−49.
(24) Shi, C.; Zhitomirsky, I. *Surf. Eng.* **2011**, *27*, 655−661.
(25) Benson, J.; Kovalenko, I.; Boukhalfa, S.; Lashmore, D.; Sanghadasa, M.; Yushin, G. *Adv. Mater.* **2013**, DOI: 10.1002/adma.2013013.
(26) Zhitomirsky, I. *Adv. Colloid Interface Sci.* **2002**, *97*, 277−315.
(27) Ohshima, H. *Colloids Surf., A* **1995**, *103*, 249−255.
(28) Taberna, P.; Simon, P.; Fauvarque, J. F. *J. Electrochem. Soc.* **2003**, *150*, A292−A300.
(29) Kudoh, Y. *Synth. Met.* **1996**, *79*, 17−22.
(30) Zhang, X.; Zhang, J.; Liu, Z.; Robinson, C. *Chem. Commun.* **2004**, 1852−1853.
(31) Hu, X.; Bao, H.; Wang, P.; Jin, S.; Gu, Z. *Polym. Int.* **2012**, *61*, 768−773.
(32) Wang, Y.; Yu, C.; Li, Z.; Zhou, D.; Chen, W.; Xue, G. *Colloid Polym. Sci.* **2009**, *287*, 1325−1330.
(33) Wang, Y.; Chen, W.; Zhou, D.; Xue, G. *Macromol. Chem. Phys.* **2009**, *210*, 936−941.

(34) Wu, G.; Katsumura, Y.; Chu, G. *Phys. Chem. Chem. Phys.* **2000**, *2*, 5602−5605.
(35) Mohanty, P.; Lee, J.; Glover, K.; Landskron, K. *Nanoscale Res. Lett.* **2011**, *6*, 61.
(36) Wu, C. *Macromolecules* **1994**, *27*, 7099−7102.
(37) De, S.; Mandal, S. *Colloids Surf. A* **2013**, *421*, 72−83.
(38) Jana, N. R.; Gearheart, L.; Murphy, C. J. *J. Phys. Chem. B* **2001**, *105*, 4065−4067.
(39) Jana, N. R.; Gearheart, L.; Murphy, C. J. *Chem. Commun.* **2001**, 617−618.
(40) Sadki, S.; Schottland, P.; Brodie, N.; Sabouraud, G. *Chem. Soc. Rev.* **2000**, *29*, 283−293.
(41) Weng, B.; Shepherd, R.; Chen, J.; Wallace, G. G. *J. Mater. Chem.* **2011**, *21*, 1918−1924.
(42) Zhitomirsky, I. *Mater. Lett.* **2000**, *42*, 262−271.
(43) Sarkar, P.; Nicholson, P. S. *J. Am. Ceram.Soc.* **1996**, *79*, 1987−2002.
(44) Shin, J.-Y.; Premkumar, T.; Geckeler, K. E. *Chem.—Eur. J.* **2008**, *14*, 6044−6048.
(45) Luo, J.; Duan, Z.; Li, H. *Phys. Status Solidi A* **2009**, *206*, 2783−2790.
(46) Guo, C.; Zuo, Y.; Zhao, X.; Zhao, J.; Xiong, J. *Surf. Coat. Technol.* **2008**, *202*, 3385−3390.
(47) Zhang, X.; Zhang, J.; Wang, R.; Liu, Z. *Carbon* **2004**, *42*, 1455−1461.
(48) Vigolo, B.; Penicaud, A.; Coulon, C.; Sauder, C.; Pailler, R.; Journet, C.; Bernier, P.; Poulin, P. *Science* **2000**, *290*, 1331−1334.
(49) Ren, X.; Pickup, P. G. *J. Electroanal. Chem.* **1994**, *372*, 289−291.
(50) Tanguy, J.; Mermilliod, N.; Hoclet, M. *J. Electrochem. Soc.* **1987**, *134*, 795−802.
(51) Feldman, B. J.; Burgmayer, P.; Murray, R. W. *J. Am. Chem. Soc.* **1985**, *107*, 872−878.
(52) Pickup, P. G.; Osteryoung, R. A. *J. Am. Chem. Soc.* **1984**, *106*, 2294−2299.